


Research Article

Photoelectric Performance Optimization of Dye-Sensitized Solar Cells Based on ZnO-TiO₂ Composite Nanofibers

Qiqi Chang ¹, Jun Xu ¹, Yijun Han ¹, Andrea Ehrmann ², Tianhong He ¹,
and Ruiping Zheng¹

¹School of Textile Science and Engineering, Tiangong University, Tianjin 300387, China

²Faculty of Engineering and Mathematics, Bielefeld University of Applied Sciences, 33619 Bielefeld, Germany

Correspondence should be addressed to Jun Xu; msdrxujun@163.com and Tianhong He; hetianhong@tiangong.edu.cn

Received 13 January 2022; Revised 29 March 2022; Accepted 5 April 2022; Published 30 April 2022

Academic Editor: P. Davide Cozzoli

Copyright © 2022 Qiqi Chang et al. This is an open access article distributed under the Creative Commons Attribution License, which permits unrestricted use, distribution, and reproduction in any medium, provided the original work is properly cited.

As the electron transport layer of dye-sensitized solar cells (DSSCs), the photoanode is an important component that affects photoelectric conversion efficiency (PCE). The commonly used material titanium dioxide (TiO₂) is difficult to prepare as nanostructures with large specific surface area, which affects dye loading and electrolyte diffusion. Herein, TiO₂ nanofibers and ZnO-TiO₂ composite nanofibers with different molar ratios are synthesized by electrospinning technology. The above nanofibers are coated on photoanodes by the doctor blade method to assemble DSSCs. The influence of the composite ratio of ZnO-TiO₂ composite nanofibers on the photoelectric performance of the assembled DSSCs is explored. The ZnO-TiO₂ composite nanofibers with a molar ratio of 1:2 have large specific surface area and porosity and have the smallest charge transfer resistance at the photoanode-electrolyte interface. The PCE of the nanofiber-modified DSSCs reaches a maximum of 3.66%, which is 56% higher than that of the TiO₂ nanofiber-modified DSSCs. The photovoltaic parameters such as open circuit voltage (V_{OC}), current density (J_{SC}), and fill factor (FF) are 0.58 V, 10.36 mA/cm², and 0.61, respectively. Proper compounding of zinc oxide (ZnO) can not only make the nanofibers absorb more dyes and enhance the light-harvesting ability but also improve the diffusion of the electrolyte and enhance the electron transport, thus successfully improving the power conversion efficiency of DSSCs.

1. Introduction

The reduction of fossil fuel resources and the emergence of numerous environmental problems have promoted the development and utilization of renewable energy [1]. Solar photovoltaic (PV) technology is one of the most promising technologies [2]. DSSCs have the excellent characteristics of simple preparation, low cost, good flexibility, and easy bending and are widely researched as the potential energy supply for intelligent wearable devices. The photoanode in DSSCs plays a role in supporting dye molecules to absorb sunlight and excite photoelectrons [3]. Improving the electron transport property of the photoanode is an effective way to improve the PCE of the DSSCs [4]. The commonly used material for photoanodes is TiO₂, which is nontoxic, environmentally friendly, low-cost, and stable. However,

the carrier transmission rate of TiO₂ is low, and it cannot be used to prepare nanostructures with large specific surface areas [5].

In order to optimize the utility of TiO₂ in the photoanode, researchers have made various attempts to improve TiO₂-based photoanodes: combining broadband gap semiconductor oxides (such as ZnO, SnO₂ [6, 7], and Nb₂O₅), metal elements (such as Cu [8], Ag [9], Zn, and Co [10, 11]), nonmetallic elements (such as N and C), rare earth elements (such as La [12] and Ce [13]), carbon materials (such as carbon dots, graphene, activated carbon, and carbon nanotubes), and multidoping (such as Cu/S [14], Al/N [15], and Cu/graphene [16]). Among many substances, ZnO has similar band gap energy and band position as TiO₂, has a variety of synthesizability, much higher electron mobility [17, 18], and lower light deactivation rate [19] than

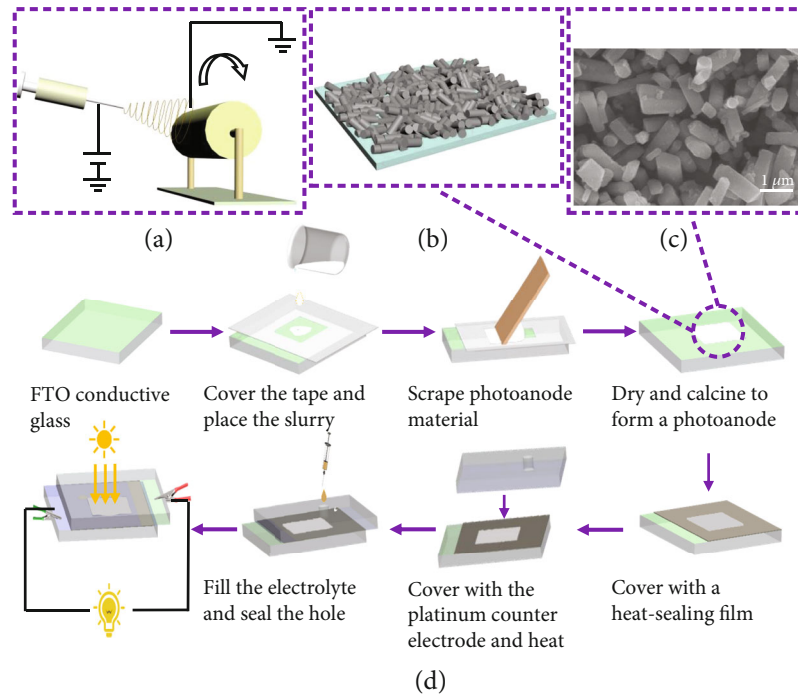


FIGURE 1: Schematic diagram of electrospinning (a), schematic diagram of fiber distribution on FTO surface (b), SEM image of short rod-like F2 composite fibers (c), and schematic diagram of DSSCs assembly (d).

TiO₂. In recent years, some reports have shown that the addition of ZnO can improve the photoelectric conversion efficiency of TiO₂-based DSSCs [20–24]. Composite nanomaterials could improve electrical conductivity, but excessive recombination would lead to catalytically active site shielding [25]. With the increase of ZnO, nonconductive Zn²⁺/dye complexes will be produced, which will reduce the rate of electron injection into TiO₂ conduction band, resulting in a low PCE of DSSCs [26, 27]. Therefore, it is very important to explore the influence of the compound ratio of the two materials on the photoelectric conversion efficiency. This work takes different molar ratios as the starting point to explore the effect of ZnO-TiO₂ composites on DSSCs.

There are many ways to prepare TiO₂ and ZnO composites, such as hydrothermal method [28–30], chemical vapor deposition method [31, 32], solution sol technology [33], solution combustion approach [34], and hot pressing method [35]. Among them, electrospinning is a simple method which can control the fiber shape, has reasonable cost, and can be used for large-scale production [36]. A large number of studies have been carried out on the electrospinning technology of TiO₂ and ZnO composites. Wang et al. [37] firstly reported the successful preparation of porous TiO₂/ZnO composite nanofibers by electrospinning in 2010. Ramos et al. [38] found that electrospinning enables the coupling of TiO₂ and ZnO and enhances the incident photon current efficiency. Boyadjiev et al. [39] employed electrospinning technology supplemented by atomic layer deposition to prepare TiO₂/ZnO and ZnO/TiO₂ core/shell composite nanofibers and found that the thinnest possible shell film has the best photocatalytic performance. Du et al. [40] reported that the PCE of DSSCs with TiO₂/ZnO core-shell nanofiber film as photoanode prepared by coaxial electrospinning

technology increased from 4.47% to 5.17%. Song et al. [41] reported that the PCE of DSSCs with TiO₂-ZnO core-shell particles prepared by coaxial electrospinning and calcination as a photoanode was 5.31%, which was an increase of 23% compared with DSSCs based on TiO₂. Nien et al. [42] employed ZnO-TiO₂ nanofibers prepared by electrospinning at a weight ratio of 3:97, as an additional layer between the TiO₂ layer and the electrolyte in the photoanode of DSSCs, and achieved the highest PCE of 6.33%. Although some promising results have been achieved in the relevant studies, the mechanism of ZnO and TiO₂ composite is unclear, and the research on composite ratio is not comprehensive. It is worth investigating the optimal doping ratio to achieve the optimal effect of TiO₂ and ZnO composite on the photoanode.

In the present study, TiO₂ nanofibers and ZnO-TiO₂ composite nanofibers with different molar ratios were designed and prepared by electrospinning technology for the fabrication of DSSCs photoanodes. The morphology and structural characteristics of the fibers and the photovoltaic performance of nanofiber-based DSSCs were analyzed to explore the application of composite fibers in the photoanode and the effect of the composite ratio on the PCE.

2. Experimental

2.1. Materials and Reagents. All solvents and reagents, unless otherwise stated, were of purest quality and used as received. Anhydrous ethanol (C₂H₆O, AR) and N,N-dimethylformamide (DMF, AR) were purchased from Tianjin Fengchuan Chemical Reagent Technology Co., Ltd. Polyvinylpyrrolidone (PVP, MW = 1300 kDa), tetrabutyl titanate (C₁₆H₃₆O₄Ti, AR), glacial acetic acid (C₂H₄O₂, AR), lithium

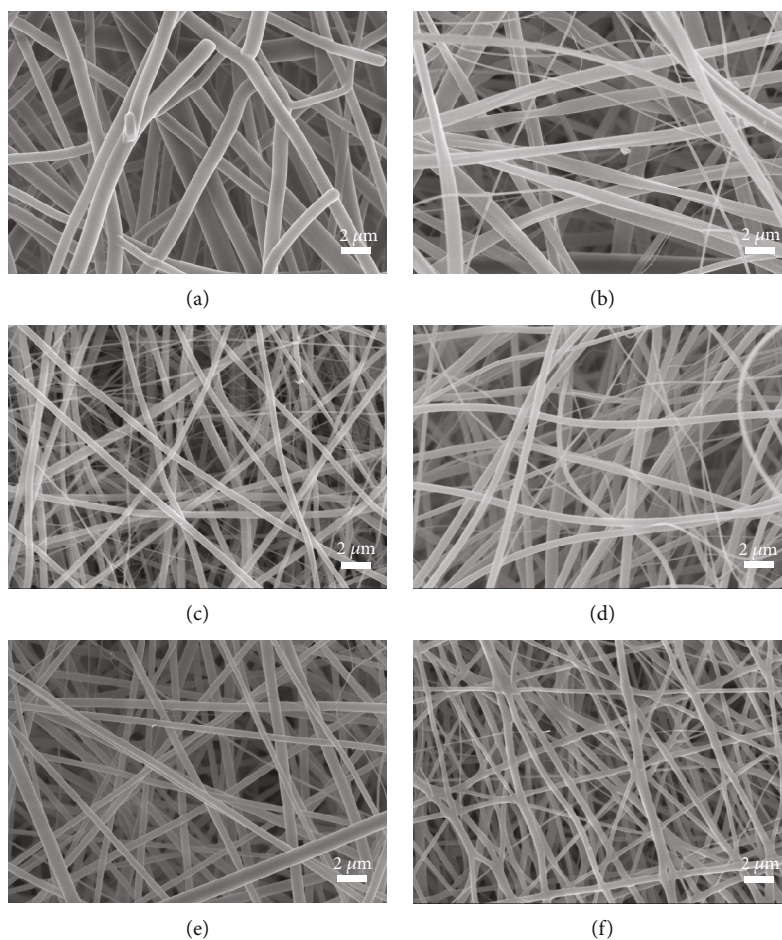


FIGURE 2: SEM images of TiO_2 precursor fibers (a) and ZnO-TiO_2 precursor fibers with molar ratios of 1:4 (b), 1:2 (c), 1:1 (d), 2:1 (e), and 4:1 (f).

iodide (LiI), iodine (I_2 , AR), acetonitrile ($\text{C}_2\text{H}_3\text{N}$, AR), ruthenium(II)bis(tetrabutylammonium) (N719 dye, AR, CAS No. 207347-46-4), ethyl cellulose, and terpineol ($\text{C}_{10}\text{H}_{18}\text{O}$, AR) were purchased from Shanghai McLean Biochemical Technology Co., Ltd. Lithium perchlorate (LiClO_4) was purchased from Aladdin Reagent (Shanghai) Co., Ltd. Zinc acetate ($\text{C}_4\text{H}_6\text{O}_4\text{Zn}\cdot 2\text{H}_2\text{O}$, AR) was purchased from Tianjin Kemeiou Chemical Reagent Co., Ltd. FTO conductive glasses (sheet resistance of 6-8 Ω) and the heat-sealing film were purchased from Liaoning Yingkou Optima New Energy Technology Co., Ltd. Deionized water was used throughout the experiment.

2.2. Preparation of Electrospinning Precursor Solution. Electrospinning precursor solution was prepared in four steps. 1.3 g of PVP and 10 ml of absolute ethanol were mixed and stirred for 1 h. Separately, 3 ml of absolute ethanol, 3 ml of glacial acetic acid, and 1.5 ml of tetrabutyl titanate were mixed and stirred for 15 minutes. The above two solutions were mixed and stirred for 30 minutes and then vacuumed to obtain a homogeneous spinning solution to form TiO_2 nanofibers. The molar ratio of ZnO and TiO_2 was designed to be 1:4, 1:2, 1:1, 2:1, and 4:1 to prepare a mixed solution of zinc acetate and DMF, which was mixed with the corresponding amount of TiO_2 spinning solution. After

ultrasonic stirring, a homogeneous spinning solution was obtained to form ZnO-TiO_2 composite nanofibers [43, 44].

2.3. Preparation of Nanofibers. As shown in Figure 1(a), the spinning solution formed a stable Taylor cone and was uniformly deposited for a certain period of time to obtain an electrospun fiber membrane. The parameters of electrospinning were as follows: propulsion speed, high voltage, and receiving distance were set to 0.8 ml/h, 15 kV, and 12 cm, respectively. The fiber membrane was vacuum dried at 80 $^\circ\text{C}$ for 4 hours, heated to 500 $^\circ\text{C}$ at the rate of 5 K/min in nitrogen atmosphere for 4 hours, and naturally cooled to room temperature. The resulting TiO_2 nanofibers and ZnO-TiO_2 nanofibers with ZnO/TiO_2 molar ratios of 1:4, 1:2, 1:1, 2:1, and 4:1 were denoted as F, F1, F2, F3, F4, and F5, respectively.

2.4. DSSC Fabrication. A schematic diagram of DSSC assembly was shown in Figure 1(d). FTO conductive glass was used as the photoanode substrate. It was first ultrasonically cleaned with acetone, ethanol, and deionized water. Then, 0.25 g of ground nanofibers, 0.5 g of ethyl cellulose, 0.5 ml of terpineol, and 5 ml of absolute ethanol were evenly mixed to form a slurry. A schematic diagram of the fiber distribution on the FTO surface and a SEM image of the short

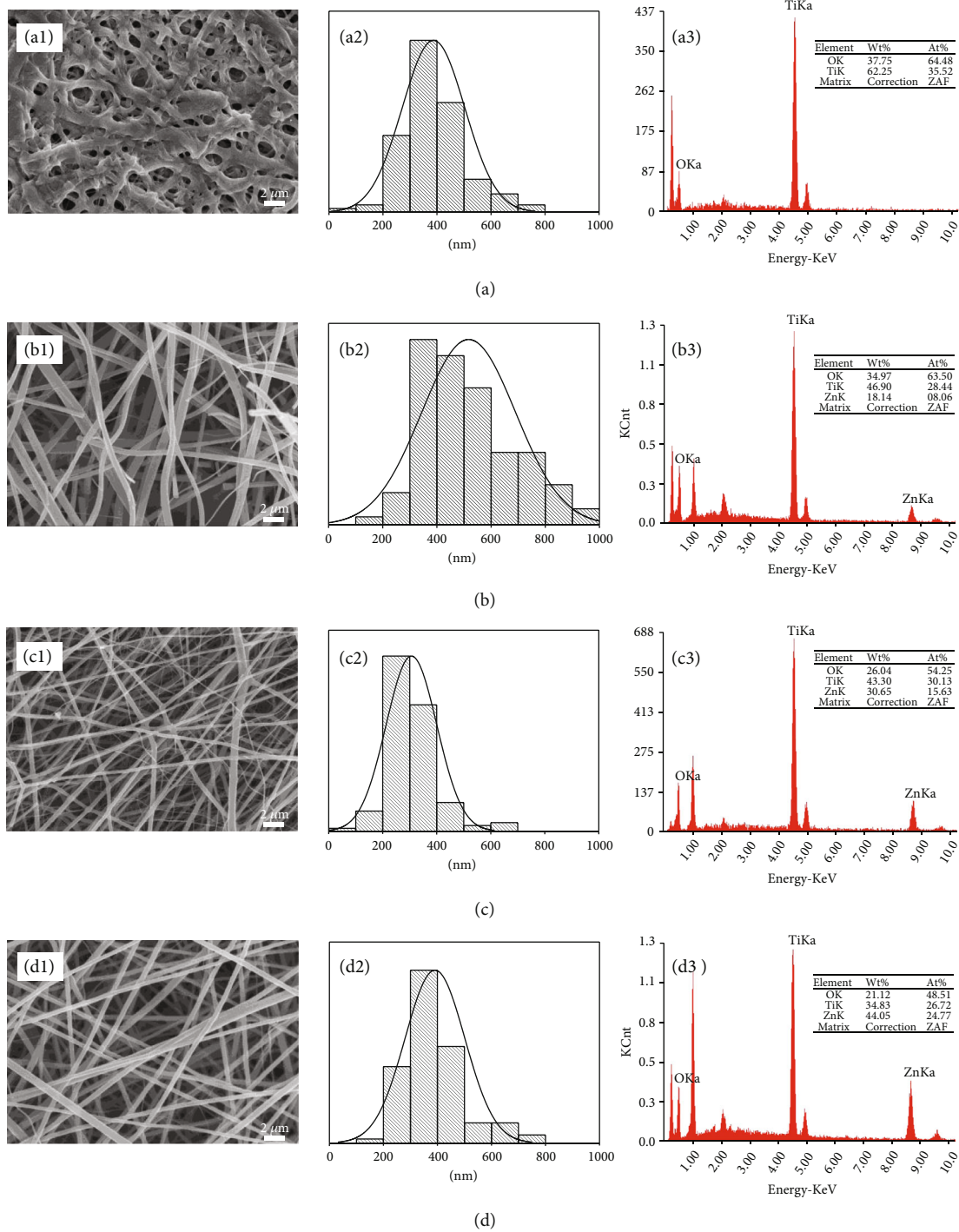


FIGURE 3: Continued.

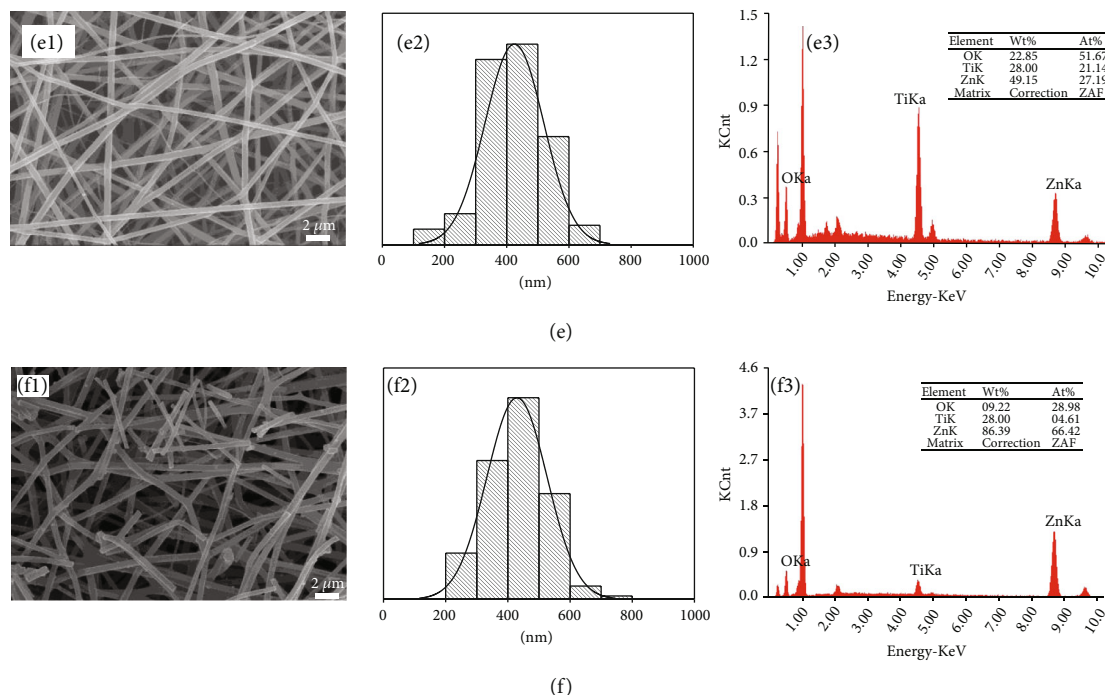


FIGURE 3: SEM images (a1)–(f1), fiber diameter distributions (a2)–(f2), EDS spectra (a3)–(f3) and element ratio charts (illustration of (a3)–(f3)) of TiO_2 nanofibers and ZnO-TiO_2 composite nanofibers with molar ratios of 1:4, 1:2, 1:1, 2:1, and 4:1.

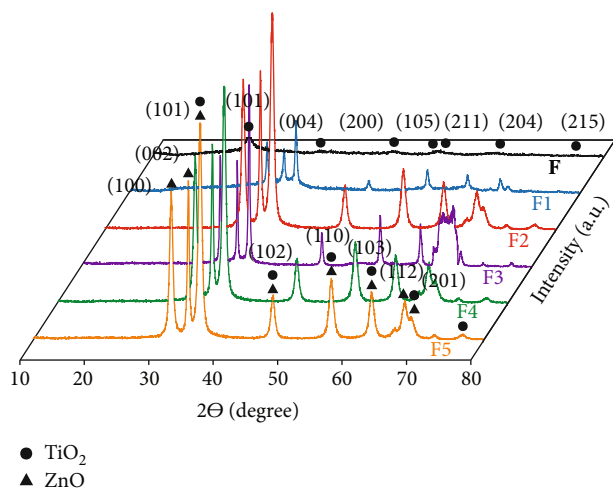


FIGURE 4: XRD patterns of TiO_2 nanofibers and ZnO-TiO_2 composite nanofibers with molar ratios of 1:4, 1:2, 1:1, 2:1, and 4:1.

rod-shaped F2 composite fibers were shown in Figures 1(b) and 1(c). The slurry was scraped and coated on FTO with $8\text{ mm} \times 8\text{ mm}$ working area with a scraper repeatedly. FTO was kept in a tubular furnace at 450°C for half an hour and then cooled down naturally. Afterward, it was taken out and soaked in dye solution (N719) in the dark for 24 hours. Dye solution was prepared by dissolving 0.074 g of N719 dye in 250 ml of absolute ethanol. Then, it was gently washed with $\text{C}_2\text{H}_6\text{O}$ and dried naturally [18, 34, 45]. A perforated heat-sealing film was placed on the surface of the photoanode conductive glass, and the photoanode was exposed. A perforated commercial platinum electrode and

the photoanode were alternately clamped and then heated at 120°C for 5 minutes to melt the heat-sealing film to seal the DSSCs. Using a needle tube, the iodine-based electrolyte was injected into the opening of the counter electrode. The electrolyte solution was prepared by dissolving 0.53 g of lithium iodide, 4.25 g of lithium perchlorate, and 1.01 g of iodine in 200 ml of acetonitrile. After filling the interlayer, the opening was sealed with quick-drying glue to complete the assembly of DSSCs.

2.5. Characterization. The morphology and elemental characteristics of the fibers were obtained with S4800 cold field emission scanning electron microscope (SEM) and the attached energy spectrometer (EDS). The crystallinity of the fibers was characterized by D8 DISCOVER X-ray diffractometer (XRD). The specific surface area and pore diameter of the fibers were measured by a BSE-PS(M) specific surface area and pore size analyzer through Brunauer-Emmett-Teller (BET) method and Barret-Joyner-Halenda (BJH) method. The electrochemical impedance spectra (EIS) and photovoltaic performance of DSSCs were measured by CHI660E electrochemical workstation and solar light simulator (100 mW/cm^2 , AM1.5G), and the test data of each test sample was not less than 5 groups.

3. Results and Discussion

3.1. SEM Analysis. As shown in Figures 2 and 3, the surface of the precursor fibers was smooth, and there were many ultrafine fibers. After calcination, the overall fibers were thinner, and some fibers were broken, branched, and curled. As the molar ratio of ZnO increased, the average fiber diameter

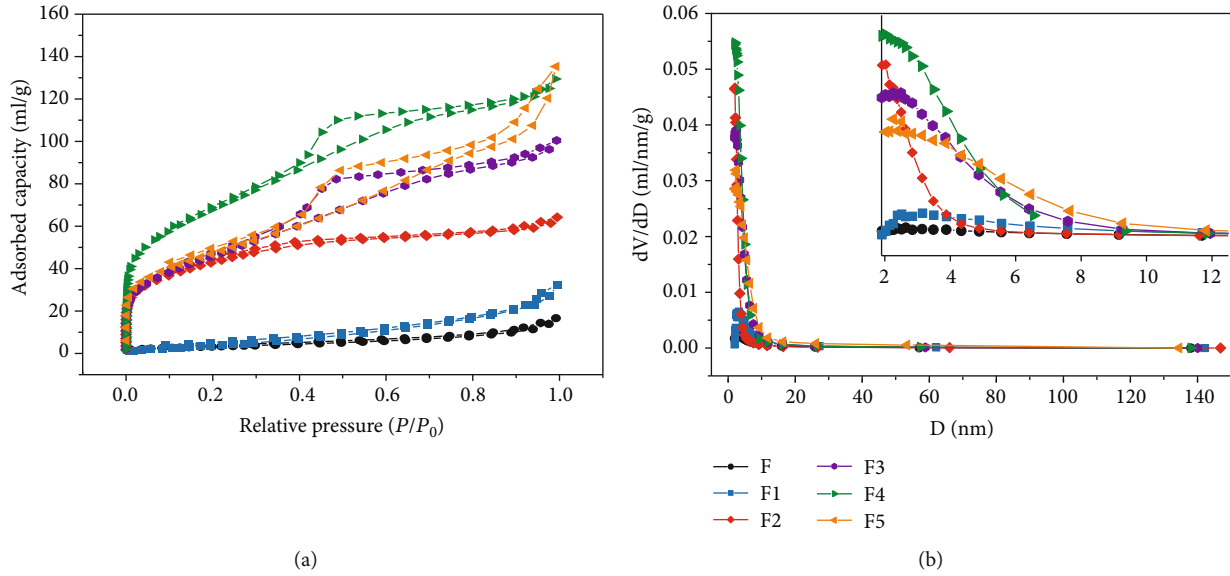


FIGURE 5: Nitrogen adsorption and desorption isotherms (a), BJH (adsorption) pore volume and pore size curves (b) of TiO_2 nanofibers and ZnO-TiO_2 composite nanofibers with molar ratios of 1 : 4, 1 : 2, 1 : 1, 2 : 1, and 4 : 1.

TABLE 1: BET results of nanofibers.

Samples	Isotherm	Specific surface area (m^2/g)	Adsorption pore volume (ml/g)	Average hole diameter (nm)
F	Type III	12.01	0.02	8.46
F1	Type III	18.17	0.05	6.49
F2	Type IV	149.65	0.07	2.88
F3	Type IV	166.82	0.15	3.63
F4	Type IV	241.59	0.18	3.41
F5	Type IV	166.81	0.19	5.00

tended to decrease, and the average diameter of all types of fibers was about 400 nm. The F2 fiber was the thinnest, while the F4 fiber exhibited the best shape and uniformity. After calcination, the fiber diameter was generally reduced and the reduction of fiber diameter showed a decreasing trend.

3.2. EDS Analysis. Qualitative and semiquantitative EDS analyses were conducted on the samples. As shown in Figure 3, TiO_2 nanofibers presented an enrichment area of Ti and contained O. The combination of mass percentage and atomic number percentage confirmed that TiO_2 nanofibers were successfully prepared. The composite nanofibers were abundant in Ti, O, and Zn elements and contained a small amount of impurity elements. With the increase in ZnO molar ratio, the weight ratio of the element Zn also increased. The relative error between the mass percentage of sample F to F4 and the theoretical calculation value was within 10%, and the relative error of F5 was within 25%.

3.3. XRD Analysis. As shown in Figure 4, the XRD pattern of TiO_2 nanofibers presented diffraction peaks at 2θ of 25.41° , 38.06° , 48.12° , 54.15° , 55.16° , 68.89° , and 75.26° , corresponding to the (101), (004), (200), (105), (211), (204), and (215) crystal planes of the TiO_2 anatase phase. In addition to the diffraction peaks of TiO_2 , the XRD pattern of ZnO-TiO_2

composite nanofibers also showed diffraction peaks of hexagonal ZnO at 31.8° , 34.4° , 36.3° , 47.5° , 56.6° , 66.4° , 67.9° , and 69.0° , corresponding to the (100), (002), (101), (102), (110), (103), (112), and (201) planes. All peaks were well matched with the standard JCPDS no: 21-1276 and 043-0002 [42, 46]. ZnO exhibited sharp diffraction peaks and good crystallinity. These results confirmed that ZnO-TiO_2 composite nanofibers were successfully prepared.

3.4. BET Analysis. Through the N_2 isotherm adsorption and desorption test on F, F1, F2, F3, F4, and F5 fibers, the nitrogen adsorption and desorption isotherms and the BJH (adsorption) pore volume and pore size curves were obtained, as shown in Figure 5. The data of the fiber-specific surface area calculated by BET multipoint method, adsorption pore volume, and average pore diameter according to BJH method were shown in Table 1. As shown in Figure 5(a), F and F1 nanofibers were difficult in the initial stage of adsorption, but self-acceleration occurred as the adsorption process progresses. Both showed weak interactions and exhibited type III isotherms. The adsorption hysteresis loop appeared in the middle section of the F2 to F5 nanofibers, indicating that it was the slit pores generated by the layered structure, corresponding to the system with capillary condensation. The isotherms of F2 to F5 nanofibers

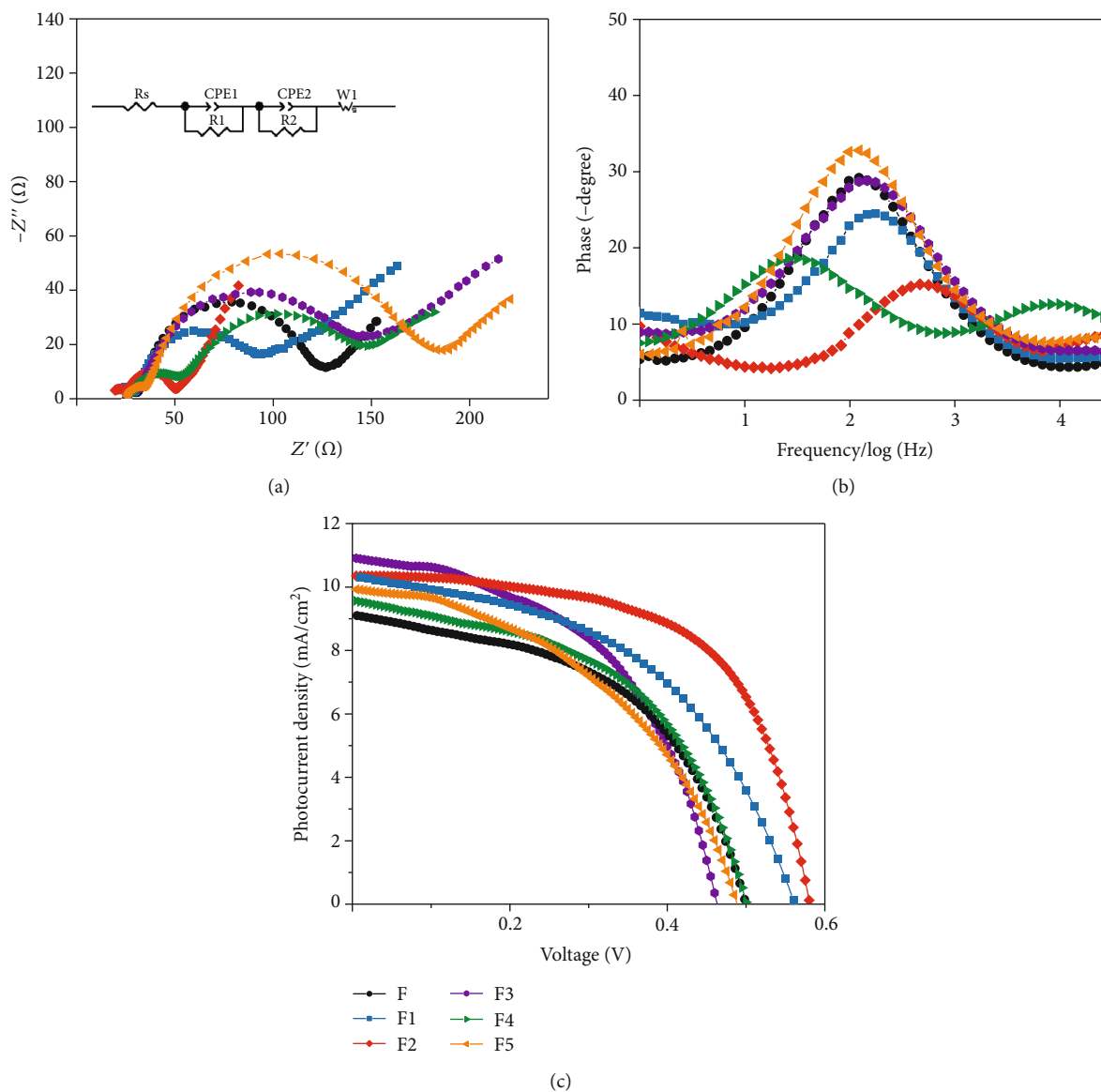


FIGURE 6: Nyquist plots along with the equivalent circuit (a), Bode plots (b), and J-V curves (c) of TiO₂ nanofibers based DSSCs and ZnO-TiO₂ composite nanofibers based DSSCs with molar ratios of 1 : 4, 1 : 2, 1 : 1, 2 : 1, and 4 : 1.

exhibited type IV isotherms with mesoporous structure. With the increase of ZnO molar ratio, the specific surface area of the composite fibers increased first and then decreased. The specific surface area of F4 nanofibers was the largest, and the difference between F2, F3, and F5 nanofibers was not large. In general, the specific surface area of the samples is positively correlated with the dye adsorption capacity. With larger specific surface area, more catalytically active sites can be exposed. As shown in Figure 5(b) and Table 1, with the increase of ZnO molar ratio, the pore volume of the composite nanofibers increased, the average pore diameter first decreased and then increased, and F2 nanofibers had the smallest average pore diameter. The line width expanded with increasing ZnO molar ratio, implying an increase in pore size distribution [46]. The pore size range of F and F1 nanofibers was 2~10 nm, while the pore size range of F2 to F5 nanofibers was 2~4 nm, 2~8 nm, 2~9 nm,

and 2~9 nm, respectively. Although F4 nanofibers had the largest surface area, there were more pores with relatively large pore sizes, and the distribution range of F2 nanofibers was the narrowest among F2 to F5, indicating that it contained the smallest pores with the largest proportion. Large porosity can reduce the electron diffusion coefficient [47], and small pore size can increase the connectivity between particles, thereby increasing the charge transport rate. The application of semiconductor photoanodes in DSSCs requires it to have extremely high porosity and surface area to adsorb a large number of dye molecules that can absorb a large number of photons and generate a large number of free electrons [34]. In conclusion, F2 nanofibers with larger specific surface area and porosity were expected to be advantageous.

3.5. EIS Analysis. The impedance of the photoanode was tested by EIS. The Nyquist and Bode plots of DSSCs

TABLE 2: EIS results and J-V results of the prepared DSSCs.

Photoanodes	R_s (Ω)	R_1 (Ω)	R_2 (Ω)	V_{OC} (V)	J_{SC} (mA/cm ²)	FF	PCE (%)
F	26.1	4.5	84.1	0.50	9.02	0.52	2.35
F1	24.0	1.6	42.2	0.56	10.27	0.49	2.84
F2	16.9	8.6	23.5	0.58	10.36	0.61	3.66
F3	25.5	3.2	88.7	0.47	11.12	0.49	2.56
F4	27.1	23.5	67.9	0.50	9.47	0.52	2.47
F5	25.3	7.2	118.5	0.49	9.98	0.45	2.20

assembled by nanofibers with different molar ratios were shown in Figure 6, and the inset was the equivalent circuit diagram of DSSCs. The impedance values were summarized in Table 2. R_1 and CPE_1 represent the charge transfer resistance and double-layer chemical capacitance of the platinum counter electrode/electrolyte, R_2 and CPE_2 represent the charge transfer resistance and double-layer chemical capacitance of the photoanode/electrolyte, and R_s is the resistance between the glass and the photoanode. With the addition of ZnO, R_s and R_2 showed a trend of first decreasing and then increasing, indicating that the addition of ZnO first increased the catalytic activity of composite nanofibers and then reduced it. When the molar ratio of ZnO to TiO_2 was 1 : 2, R_2 was the smallest, which was 23.5 Ω . Lower R_2 represents higher catalytic activity [48–50]. In other words, F2 nanofibers can carry out the redox reaction at the interface between photoanode material and electrolyte fastest. In the Bode plot, the intermediate frequency peak represents the charge transfer process of injected electrons [51]. With the increase in ZnO molar ratio, the phase value first decreased and then increased. F2 nanofibers exhibited the lowest phase value and the phase peak of F4 nanofibers shifted significantly to the low-frequency region. Combining the results of Nyquist and Bode plots, F2 nanofibers had the highest catalytic activity, and its redox reaction was faster at the interface between photoanode and electrolyte, which can promote electron transport.

3.6. J-V Characteristics. Figure 6 showed the J-V characteristics of nanofibers, and the detailed parameters were given in Table 2. The composite of ZnO improved the band gap of composite nanofibers. Compared with DSSCs based on TiO_2 nanofibers, DSSCs based on composite fibers showed higher V_{OC} and higher J_{SC} . The V_{OC} of DSSCs based on ZnO- TiO_2 composite fibers with a molar ratio of 1 : 2 increased from 0.50 V to 0.58 V, the J_{SC} increased from 9.02 mA/cm² to 10.36 mA/cm², the FF increased from 0.52 to 0.61, and the highest photoelectric conversion efficiency reached 3.66%, which was an increase of 56% compared with DSSCs based on TiO_2 nanofibers. The optimization of DSSC performance can be explained as follows: first, the one-dimensional nanomaterials prepared by electrospinning originally had a large specific surface area. By adding appropriate ZnO, the composite nanofibers got increased porosity to absorb more dyes and enhance the light capture ability. In addition, the higher porosity improved the diffusion of electrolyte to the semiconductor and enhanced the redox ability of dye molecules, which produced more electrons in the photoanode. Therefore, more

current could be generated by electron transmission to improve the performance of DSSCs.

4. Conclusions

A DSSC is a multicomponent whole. In order to improve PCE, photoanode material with large specific surface area and large porosity is expected. On the one hand, it is necessary to provide a place for attaching dye sensitizers. On the other hand, it is also necessary to provide a channel for electrolyte diffusion. Second related to the photoanode is sensitizers and electrolytes, whose intrinsic properties such as adhesion to the photoanode material and electron transport rate have a direct impact on the PCE of DSSCs.

In this work, electrospinning as a simple production method is used to prepare photoanode materials with large specific surface area nanostructures. The achievements of this study are summarized as follows. First, this research successfully explored the preparation method of ZnO- TiO_2 composite nanofibers, an ideal component of DSSCs photoanode semiconductor. Second, it is proved that the ZnO- TiO_2 composite nanofibers with a molar ratio of 1 : 2 had the best porosity and specific surface area, which could absorb more dyes to enhance the light-harvesting ability and improve the diffusion of electrolytes to enhance electron transport. Finally, it is concluded that the ZnO- TiO_2 nanofibers modified DSSCs with a molar ratio of 1 : 2 had the lowest impedance at the photoanode-electrolyte interface and showed the highest PCE of 3.66%, which was 56% higher than that of the TiO_2 nanofiber modified DSSCs. The above results provide important supporting data for interpreting the internal mechanism of TiO_2 -based composite photoanodes. The characteristics of dye sensitized solar cell enable its great prospects in application of intermittent power supply, small-scale power supply, and micro energy storage. Low-power components such as display screens or sensors can be widely applied with dye sensitized solar cell.

Data Availability

The research data used to support the findings of this study are included in the article.

Conflicts of Interest

The authors declare no conflict of interest.

Authors' Contributions

Qiqi Chang and Jun Xu contributed equally to this work.

Acknowledgments

The authors would like to thank the Analytical & Testing Center of Tiangong University for their work on cold-field-emission scanning electron microscopy, energy dispersive spectroscopy, and X-ray diffraction.

References

- [1] M. Saleem, M. Irfan, S. Tabassum et al., "Experimental and theoretical study of highly porous lignocellulose assisted metal oxide photoelectrodes for dye-sensitized solar cells," *Arabian Journal of Chemistry*, vol. 14, no. 2, p. 102937, 2021.
- [2] Z. Chamanzadeh, V. Ansari, and M. Zahedifar, "Investigation on the properties of La-doped and Dy-doped ZnO nanorods and their enhanced photovoltaic performance of dye-sensitized solar cells," *Optical Materials*, vol. 112, 2021.
- [3] C. Karam, R. Habchi, S. Tingry, P. Miele, and M. Bechelany, "Design of multilayers of urchin-like ZnO nanowires coated with TiO₂ nanostructures for dye-sensitized solar cells," *Acs Applied Nano Materials*, vol. 1, no. 7, pp. 3705–3714, 2018.
- [4] J. C. Chou, C. C. Ko, J. X. Chang et al., "Dye-sensitized solar cells using aluminum-doped zinc oxide/titanium dioxide photoanodes in parallel," *Energies*, vol. 12, no. 18, article 3469, 2019.
- [5] Q. Zhang, Q. S. W. Hou, and C. Y. Li, "Titanium dioxide-coated zinc oxide nanorods as an efficient photoelectrode in dye-sensitized solar cells," *Nanomaterials*, vol. 10, no. 8, article 1598, 2020.
- [6] A. A. Qureshi, S. Javed, H. M. A. Javed et al., "Facile formation of SnO₂-TiO₂ based photoanode and Fe₃O₄@rGO based counter electrode for efficient dye-sensitized solar cells," *Materials Science in Semiconductor Processing*, vol. 123, article 105545, 2021.
- [7] B. Pham, D. Willinger, N. K. McMillan et al., "Tin(IV) oxide nanoparticulate films for aqueous dye-sensitized solar cells," *Solar Energy*, vol. 224, pp. 984–991, 2021.
- [8] A. A. Qureshi, S. Javed, H. M. Javed, A. Akram, M. Jamshaid, and A. Shaheen, "Strategic design of Cu/TiO₂-based photoanode and rGO-Fe₃O₄-based counter electrode for optimized plasmonic dye-sensitized solar cells," *Optical Materials*, vol. 109, article 110267, 2020.
- [9] S. Rajkumar, M. R. Venkatraman, K. Suguna, P. Karuppasamy, M. S. Pandian, and P. Ramasamy, "Synthesis of Ag-incorporated TiO₂ nanoparticles by simple green approach as working electrode for dye-sensitized solar cells," *Journal of Materials Science-Materials in Electronics*, vol. 33, no. 8, pp. 4965–4973, 2022.
- [10] I. Ahmad, R. Jafer, S. M. Abbas et al., "Improving energy harvesting efficiency of dye sensitized solar cell by using cobalt-rGO co-doped TiO₂ photoanode," *Journal of Alloys and Compounds*, vol. 891, 2022.
- [11] R. Krishnapriya, C. Nizamudeen, B. Saini, M. S. Mozumder, R. K. Sharma, and A. H. I. Mourad, "MOF-derived Co²⁺-doped TiO₂ nanoparticles as photoanodes for dye-sensitized solar cells," *Scientific Reports*, vol. 11, no. 1, 2021.
- [12] M. I. Khan, B. Mehmood, M. A. Naeem et al., "Investigations the structural, optical and photovoltaic properties of La doped TiO₂ photoanode based dye sensitized solar cells," *Optical Materials*, vol. 122, article 111610, 2021.
- [13] M. I. Khan, A. Suleman, M. S. Hasan et al., "Effect of Ce doping on the structural, optical, and photovoltaic properties of TiO₂ based dye-sensitized solar cells," *Materials Chemistry and Physics*, vol. 274, article 125177, 2021.
- [14] A. Gupta, K. Sahu, M. Dhonde, and V. V. S. Murty, "Novel synergistic combination of Cu/S co-doped TiO₂ nanoparticles incorporated as photoanode in dye sensitized solar cell," *Solar Energy*, vol. 203, pp. 296–303, 2020.
- [15] K. S. Dhonde, M. Dhonde, and V. V. S. Murty, "Novel synergistic combination of Al/N Co-doped TiO₂ nanoparticles for highly efficient dye-sensitized solar cells," *Solar Energy*, vol. 173, pp. 551–557, 2018.
- [16] M. Dhonde, K. Sahu, and V. V. S. Murty, "Cu-doped TiO₂ nanoparticles/graphene composites for efficient dye-sensitized solar cells," *Solar Energy*, vol. 220, pp. 418–424, 2021.
- [17] I. Gonzalez-Valls and M. Lira-Cantu, "Vertically-aligned nanostructures of ZnO for excitonic solar cells: a review," *Energy & Environmental Science*, vol. 2, no. 1, pp. 19–34, 2009.
- [18] S. Kannan, N. P. Subiramaniam, and S. U. Lavanisadevi, "Dye-sensitized solar cells based on TiO₂ nanoparticles-decorated ZnO nanorod arrays for enhanced photovoltaic performance," *Journal of Materials Science: Materials in Electronics*, vol. 31, no. 7, pp. 3705–3714, 2020.
- [19] Z. Chamanzadeh, M. Noormohammadi, and M. Zahedifar, "Enhanced photovoltaic performance of dye sensitized solar cell using TiO₂ and ZnO nanoparticles on top of free standing TiO₂ nanotube arrays," *Materials Science in Semiconductor Processing*, vol. 61, pp. 107–113, 2017.
- [20] T. S. Senthil, N. Muthukumarasamy, and M. Kang, "Applications of highly ordered paddle wheel like structured ZnO nanorods in dye sensitized solar cells," *Materials Letters*, vol. 102–103, pp. 26–29, 2013.
- [21] M. Rani and S. K. Tripathi, "Electron transfer properties of organic dye sensitized ZnO and ZnO/TiO₂ photoanode for dye sensitized solar cells," *Renewable & Sustainable Energy Reviews*, vol. 61, pp. 97–107, 2016.
- [22] S. J. Li, Y. Lin, W. W. Tan et al., "Preparation and performance of dye-sensitized solar cells based on ZnO-modified TiO₂ electrodes," *International Journal of Minerals Metallurgy and Materials*, vol. 17, no. 1, pp. 92–97, 2010.
- [23] L. Q. Zhang, S. Zhou, F. S. Cai, and Z. Yuan, "ZnO/TiO₂ composite photoanodes for efficient dye-sensitized solar cells," *Functional Materials Letters*, vol. 7, no. 4, p. 1450039, 2014.
- [24] J. S. Jeong, B. H. Choe, J. H. Lee, J. J. Lee, and W. Y. Choi, "ZnO-coated TiO₂ nanotube arrays for a photoelectrode in dye-sensitized solar cells," *Journal of Electronic Materials*, vol. 43, no. 2, pp. 375–380, 2014.
- [25] S. Maitra, S. Halder, T. Maitra, and S. Roy, "Superior light absorbing CdS/vanadium sulphide nanowalls@TiO₂ nanorod ternary heterojunction photoanodes for solar water splitting," *New Journal of Chemistry*, vol. 45, no. 16, pp. 7353–7367, 2021.
- [26] Q. Zhang and C. Y. Li, "TiO₂ coated ZnO nanorods by mist chemical vapor deposition for application as photoanodes for dye-sensitized solar cells," *Nanomaterials*, vol. 9, no. 9, p. 1339, 2019.
- [27] A. Amini, M. S. Zakerhamidi, and S. Khorram, "Treatment of the ZnO and TiO₂ Thin Films by Electric Field in Plasma Sheath to Improve the Metal-Dye Electronic Coupling in

- Dye-Sensitized Solar Cells,” *Surfaces and Interfaces*, vol. 23, article 101028, 2021.
- [28] B. B. Çırak, Ç. Eden, Y. Erdoğan et al., “The enhanced light harvesting performance of dye-sensitized solar cells based on ZnO nanorod-TiO₂ nanotube hybrid photoanodes,” *Optik*, vol. 203, article 163963, 2020.
- [29] Q. L. Ma, S. Q. Ma, and Y. M. Huang, “Enhanced photovoltaic performance of dye sensitized solar cell with ZnO nanohoneycombs decorated TiO₂ photoanode,” *Materials Letters*, vol. 218, pp. 237–240, 2018.
- [30] S. Kerli, O. Akgul, and U. Alver, “ZnO/TiO₂ particles and their solar cell application,” in *9th International Physics Conference of the Balkan-Physical-Union (BPU)*, Istanbul, Turkey, 2015.
- [31] L. Sheng, G. Li, W. D. Zhang, and K. Wang, “Full-stainless steel mesh dye-sensitized solar cells based on core-shell ZnO/TiO₂ nanorods,” *Optik*, vol. 184, pp. 90–97, 2019.
- [32] Z. J. T. Zhang, M. He, N. Q. Fu, J. Li, and X. Yin, “Facile one-step synthesis of highly branched ZnO nanostructures on titanium foil for flexible dye-sensitized solar cells,” *Nanoscale*, vol. 6, no. 8, pp. 4211–4216, 2014.
- [33] K. A. Bhatti, M. I. Khan, M. Saleem, F. Alvi, R. Raza, and S. Rehman, “Analysis of multilayer based TiO₂ and ZnO photoanodes for dye-sensitized solar cells,” *Materials Research Express*, vol. 6, no. 7, 2019.
- [34] H. A. Deepa, G. M. Madhu, and V. Venkatesham, “Performance evaluation of DSSC’s fabricated employing TiO₂ and TiO₂-ZnO nanocomposite as the photoanodes,” *Materials Today: Proceedings*, vol. 46, no. 10, pp. 4579–4586, 2021.
- [35] M. S. H. Choudhury, N. Kishi, and T. Soga, “Compression of ZnO nanoparticle films at elevated temperature for flexible dye-sensitized solar cells,” *Journal of Alloys and Compounds*, vol. 656, pp. 476–480, 2016.
- [36] Z. Arifin, S. Hadi, H. N. Jati, and S. D. Prasetyo, “Effect of electrospinning distance to fabricate ZnO nanofiber as photoanode of dye-sensitized solar cells,” *AIP Conference Proceedings*, vol. 2217, no. 1, p. 030095, 2020.
- [37] H. Y. Wang, Y. Yang, X. A. Li, L. J. Li, and C. Wang, “Preparation and characterization of porous TiO₂/ZnO composite nanofibers via electrospinning,” *Chinese Chemical Letters*, vol. 21, no. 9, pp. 1119–1123, 2010.
- [38] P. G. Ramos, E. Flores, L. A. Sánchez et al., “Enhanced photoelectrochemical performance and photocatalytic activity of ZnO/TiO₂ nanostructures fabricated by an electrostatically modified electrospinning,” *Applied Surface Science*, vol. 426, pp. 844–851, 2017.
- [39] S. I. Boyadjiev, O. Kéri, P. Bárdos et al., “TiO₂/ZnO and ZnO/TiO₂ core/shell nanofibers prepared by electrospinning and atomic layer deposition for photocatalysis and gas sensing,” *Applied Surface Science*, vol. 424, pp. 190–197, 2017.
- [40] P. Du, L. Song, J. Xiong et al., “Coaxial electrospun TiO₂/ZnO core-sheath nanofibers film: novel structure for photoanode of dye-sensitized solar cells,” *Electrochimica Acta*, vol. 78, pp. 392–397, 2012.
- [41] L. Song, Q. Jiang, P. Du, Y. Yang, J. Xiong, and C. Cui, “Novel structure of TiO₂-ZnO core shell rice grain for photoanode of dye-sensitized solar cells,” *Journal of Power Sources*, vol. 261, pp. 1–6, 2014.
- [42] Y. H. Nien, G. M. Hu, M. Rangasamy et al., “Investigation of dye-sensitized solar cell with photoanode modified by TiO₂-ZnO nanofibers,” *IEEE Transactions on Semiconductor Manufacturing*, vol. 33, no. 2, pp. 295–301, 2020.
- [43] R. L. Liu, H. Y. Ye, X. P. Xiong, and H. Liu, “Fabrication of TiO₂/ZnO composite nanofibers by electrospinning and their photocatalytic property,” *Materials Chemistry and Physics*, vol. 121, no. 3, pp. 432–439, 2010.
- [44] C. G. Lee, K. H. Na, W. T. Kim, D. C. Park, W. H. Yang, and W. Y. Choi, “TiO₂/ZnO nanofibers prepared by electrospinning and their photocatalytic degradation of methylene blue compared with TiO₂ nanofibers,” *Applied Sciences-Basel*, vol. 9, no. 16, p. 3404, 2019.
- [45] K. Pugazhendhi, B. Praveen, D. J. Sharmila et al., “Plasmonic TiO₂/Al@ZnO nanocomposite-based novel dye-sensitized solar cell with 11.4% power conversion efficiency,” *Solar Energy*, vol. 215, pp. 443–450, 2021.
- [46] A. Zatirostami, “Fabrication of dye-sensitized solar cells based on the composite TiO₂ nanoparticles/ZnO nanorods: investigating the role of photoanode porosity,” *Materials Today Communications*, vol. 26, article 102033, 2021.
- [47] D. Cao, A. Wang, X. Yu et al., “Room-temperature preparation of TiO₂/graphene composite photoanodes for efficient dye-sensitized solar cells,” *Journal of Colloid and Interface Science*, vol. 586, pp. 326–334, 2021.
- [48] L. X. Song, P. P. Chen, Z. W. Li et al., “Flexible carbon nanotubes/TiO₂/C nanofibrous film as counter electrode of flexible quasi-solid dye-sensitized solar cells,” *Thin Solid Films*, vol. 711, article 138307, 2020.
- [49] Y. H. Nien, G. M. Hu, M. Rangasamy et al., “Investigation on photoanode modified with TiO₂-ZnO-Ag nanofibers in dye-sensitized solar cell under different intensities of illuminations,” *IEEE Transactions on Electron Devices*, vol. 67, no. 11, pp. 4983–4989, 2020.
- [50] J. C. Chou, C. C. Ko, P. Y. Kuo, C. H. Lai, Y. H. Nien, and J. X. Chang, “Fabrication of dye-sensitized solar cells using zinc oxide nanorod-modified titanium dioxide photoanode,” *IEEE Transactions on Nanotechnology*, vol. 18, pp. 553–561, 2019.
- [51] J. J. Huang, C. K. Wu, and C. F. Hsu, “Characterization of LPD-TiO₂ compact layer in ZnO nano-rods photoelectrode for dye-sensitized solar cell,” *Applied Physics a-Materials Science & Processing*, vol. 123, no. 12, 2017.